THE JOURNAL OF PHYSICAL CHEMISTRY C

pubs.acs.org/JPCC Article

First-Principles Screening of Lead-Free Mixed-Anion Perovskites for Photovoltaics

Xin Mao, Ke-Li Han, Wei-Qiao Deng, and Lei Sun*

Cite This: J. Phys. Chem. C 2020, 124, 1303−1308 Read Online

ACCESS | Metrics & More | Article Recommendations | Supporting Information

ABSTRACT: Organic−inorganic hybrid lead perovskites have made rapid progress in photovoltaic fields. However, the toxicity and poor long-term stability of these materials still limit their further commercial application. Herein, we proposed a system of lead-free mixed-anion perovskites in which a chalcogen element is incorporated into the perovskite octahedrons to improve the system stability. We performed first-principles calculations of the band gaps of 192 lead-free mixed-anion perovskites belonging to the class of $ABX'X''_2$ where A = Cs^+, $CH_3NH_3^+$, and $HC(NH_2)_2^+$; B = Ga^{3+}, In^{3+}, Sb^{3+}, and Bi^{3+}; X′ = O^{2-}, S^{2-}, Se^{2-}, and Te^{2-}, and X″ = F^-, Cl^-, Br^-, and I^-. The band gap shows a linear relationship with the average anion electronegativity. The contribution of anions to the band-edge states is related to electron affinity and structure parameters. Considering multiple factors forming perovskites, we screened out a promising candidate, $CsInOBr_2$, with a suitable band gap (1.3 eV) for application in photovoltaics.

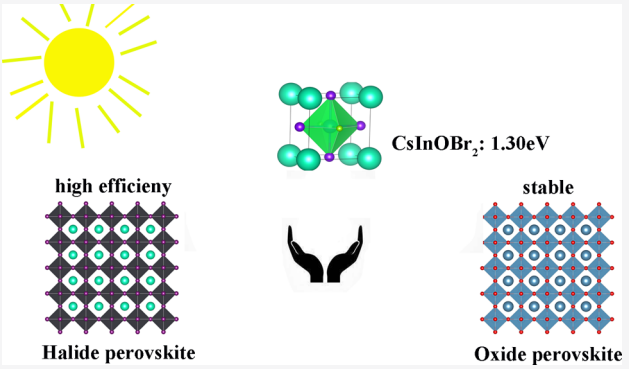

INTRODUCTION

During recent decades, three-dimensional (3D) lead halide perovskites have received enormous attention in solar cells due to their outstanding photovoltaic performance with a new exciting record power conversion efficiency of 25.2%.[1−8] Although this tremendous success makes perovskite candidates next-generation solar cells, the inherent toxicity of lead (Pb) and the poor long-term stability remain major obstacles for commercial applications.[9−18] The requirements for commercial materials to have high performance and be environmentally friendly motivate the exploration of stable, lead-free perovskites.

It is known that high electronic dimensionality resulting from the corner-shared connection of octahedral halide units contributes to the superior photovoltaic properties of 3D lead perovskites.[19] To maintain high electronic dimensionality, on the one hand, divalent elements, for example, Sn and Ge, which belong to the same group in the periodic table as Pb, have been considered primary alternatives. However, both of them are easily oxidized, leading to poor performance for 3D Sn-based and Ge-based perovskite solar cells.[20−22] On the other hand, 3D double perovskites with the formula Cs_2AgBiX_6 (X = Br, Cl) have been widely explored due to their good stability. However, their band gap is not ideal for photovoltaic applications.[23,24] Thus, searching alternatives for lead perovskites with ideal band gaps and good stability is still ongoing.

In this work, we focus on new emerging 3D mixed-anion perovskites[25,26] in which both chalcogen and halogen elements contribute to the vertexes of the octahedral units. Incorporation of chalcogen elements will help to improve the stability issue caused by dissociating halide salts in the presence of moisture.[25,26] By using computational simulation based on first principles, we achieved high-throughput screening of mixed-anion lead-free perovskites for photovoltaic applications. The band gaps of 192 mixed-anion perovskites with a formula of $ABX'X''_2$ (Figure 1) were calculated by using the DFT-GLLB-SC method, which has been shown to yield reasonable band gaps at a minimal cost for perovskites.[27−29] In this formula, A represents Cs, MA (methylammonium, CH_3NH_3), or FA (formamidinium, H_2NCHNH_2); B represents Ga, In, Sb, or Bi; X′ represents O, S, Se, or Te; and X″ represents F, Cl, Br, or I.

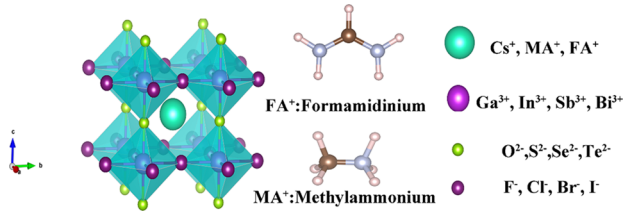

Figure 1. Crystal structure studied in this work. The organic molecules are shown in the middle.

Received: October 31, 2019
Revised: December 4, 2019
Published: December 21, 2019

https://dx.doi.org/10.1021/acs.jpcc.9b10217
J. Phys. Chem. C 2020, 124, 1303−1308

The influence of chalcogen and halogen anions on band gaps was systematically investigated in terms of different factors, including electronegativity and density of states. Considering the tolerance, octahedral factor, and stability, we screened out a promising photovoltaic candidate, $CsInOBr_2$, with a suitable band gap of 1.30 eV.

COMPUTATIONAL METHODS

In this study, all structural optimizations are based on density functional theory (DFT) methods as performed in the Vienna ab initio simulation package (VASP) by considering the generalized gradient approximation (GGA) and the Perdew–Burke–Ernzerhof (PBE) exchange-correlation functional.[33,34] The projector-augmented wave method (PAW) is applied to describe the interaction between the electrons and ions.[35] The Monkhorst–Pack k point sampling used in geometry optimization and electronic property calculation is $9 \times 9 \times 9$ and $14 \times 14 \times 14$. The cutoff energy for the plane wave functions is set to 500 eV. As for the convergence criteria of lattice relaxation and self-consistent calculations, the Hellmann–Feynman force is less than 0.01 eV/Å, and the threshold of the total energy change is set to 10^{-5} eV. The initial crystal phase for mixed-anion perovskites is set to be cubic. Spin–orbit coupling (SOC) is also calculated by using VASP software since it has been verified to have a strong relativistic correction on heavy atoms.[28,36]

It is known that standard DFT calculations with a Kohn–Sham band gap always seriously underestimate actual band gaps.[37] The general solution is the use of a hybrid functional or many-body methods.[38] Although these methods can give a more accurate band gap value, the computation time is too large, which is not appropriate for materials screening. We use the GLLB-SC model potential method implemented in the GPAW code[42] to predict the band gaps of all the optimized perovskite structures and calculate the band structure. In this work, we use the GLLB-SC model potential method, which has been shown to give reasonable results at a minimal cost to predict the band gaps of the optimized perovskite structures.[39−42] In this method, excess exchange-correlation energy (Δ_{xc}) is considered based on the Kohn–Sham band gap to obtain the quasiparticle band gap, which includes two parts: the Kohn–Sham band gap E_{gap}^{KS} and exchange-correlation energy Δ_{xc}. Besides, for accurate description of band gaps, spin–orbit coupling (SOC) calculations are also considered in our calculation as Δ_{SOC}, which can be obtained from the VASP calculation. The band structure of $CsInOBr_2$ is calculated with the GLLB-SC functional implemented in GPAW.

$$E_g = E_{gap}^{KS} + \Delta_{xc} - \Delta_{soc}$$

For the contribution of different anions on valence band maximum, we calculate the projection of each band on the orbitals of anions with VASP.

Ab initio molecular dynamics (AIMD) simulations were performed to confirm thermal stability of the selected materials, which is in supercells of $3 \times 3 \times 3$ of a unit cell. The entire MD simulation lasted 1 ps with a step of 0.5 fs. The temperature was controlled at 300 K with the canonical ensemble, which is simulated using the algorithm of Nosé.

The formation energy was calculated by

$$E_{formation} = \frac{1}{N}E_{tot}(CsInOBr_2) - E_{tot}^{solid}(Cs) - E_{tot}^{solid}(In) - \frac{1}{2}E_{tot}^{gas}(O_2) - E_{tot}^{liquid}(Br_2)$$

where $E_{formation}$ is the total energy of a supercell with N $CsInOBr_2$ formula units and E_{tot} is the total energy of the constituent elements in their solid or gas forms. Spin polarization was considered for the calculation of O_2 gas and Br_2 liquid.

The decomposition energy was calculated by considering the following deposition reactions

$$CsInOBr_2 \rightarrow CsBr + 1/2\ O_2 + InBr \quad (1)$$

$$CsInOBr_2 \rightarrow 1/6\ (3Cs_2O + In_2O_3 + 4InBr_3) \quad (2)$$

$$CsInOBr_2 \rightarrow CsBr + 1/3\ In_2O_3 + 1/3\ InBr_3 \quad (3)$$

Hence, the decomposition energy was calculated as follows

$$E_{decomposition} = [E_{tot}(CsBr) + 1/2\ E_{tot}(O_2) + E_{tot}(InBr)] - E_{tot}(CsInOBr_2)$$

$$E_{decomposition} = 1/6\ [3E_{tot}(Cs_2O) + E_{tot}(In_2O_3) + 4E_{tot}(InBr_3)] - E_{tot}(CsInOBr_2)$$

$$E_{decomposition} = 1/3\ [3E_{tot}(CsBr) + E_{tot}(In_2O_3) + E_{tot}(InBr_3)] - E_{tot}(CsInOBr_2)$$

RESULTS AND DISCUSSION

Band gap is the most important parameter that determines the performance of photovoltaic materials.[30] Accordingly, we first calculated the band gaps of 192 lead-free perovskites. To maintain the network of halide octahedrons, 1/3 of the vertexes were replaced by chalcogen elements, resulting in a formula of $ABX'X''_2$ where A is Cs^+, MA^+, or FA^+; B is Ga^{3+}, In^{3+}, Sb^{3+}, or Bi^{3+}; X′ is O^{2-}, S^{2-}, Se^{2-}, or Te^{2-}; and X″ is F^-, Cl^-, Br^-, or I^-. As shown in Figure 2, the band gaps of these selected perovskites span a range from 0 to approximately 7 eV. Most of the Cs-based compounds are metallic, with band gaps approaching zero. Most of the MA-based perovskites and some of the FA-based perovskites exhibit semiconductivity

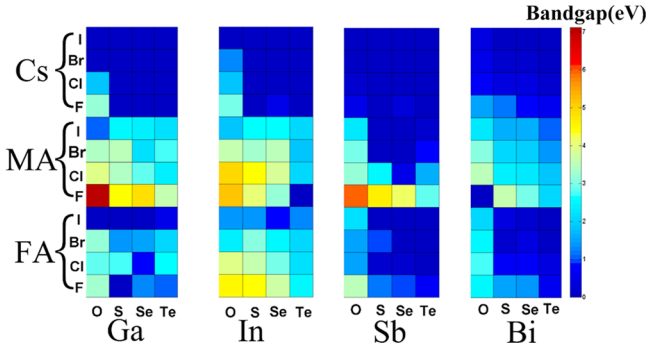

Figure 2. Calculated band gaps of 192 mixed-anion perovskites. Each square represents a compound, and the color represents the corresponding band gap. The larger letters on the left are A ions, and the smaller letters are X″ ions. The larger letters below are B ions, and the smaller letters are X′ ions.

https://dx.doi.org/10.1021/acs.jpcc.9b10217
J. Phys. Chem. C 2020, 124, 1303−1308

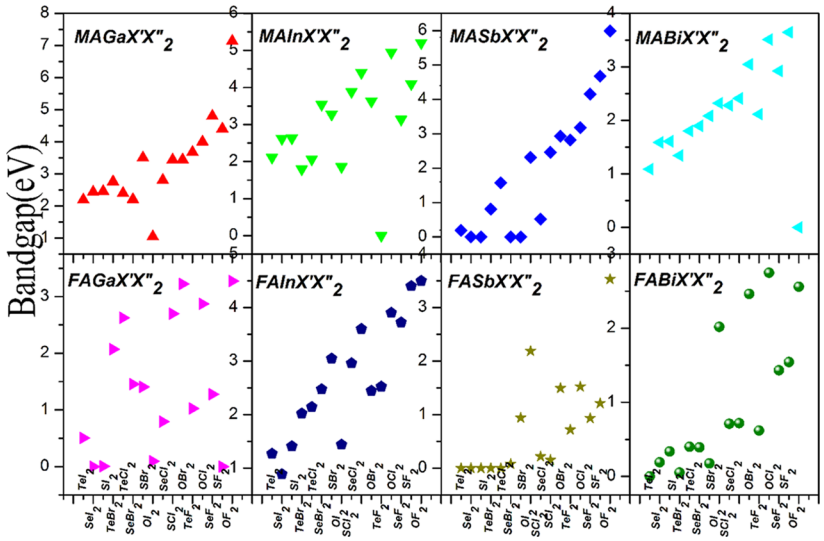

Figure 3. Band gaps as a function of average electronegativity.

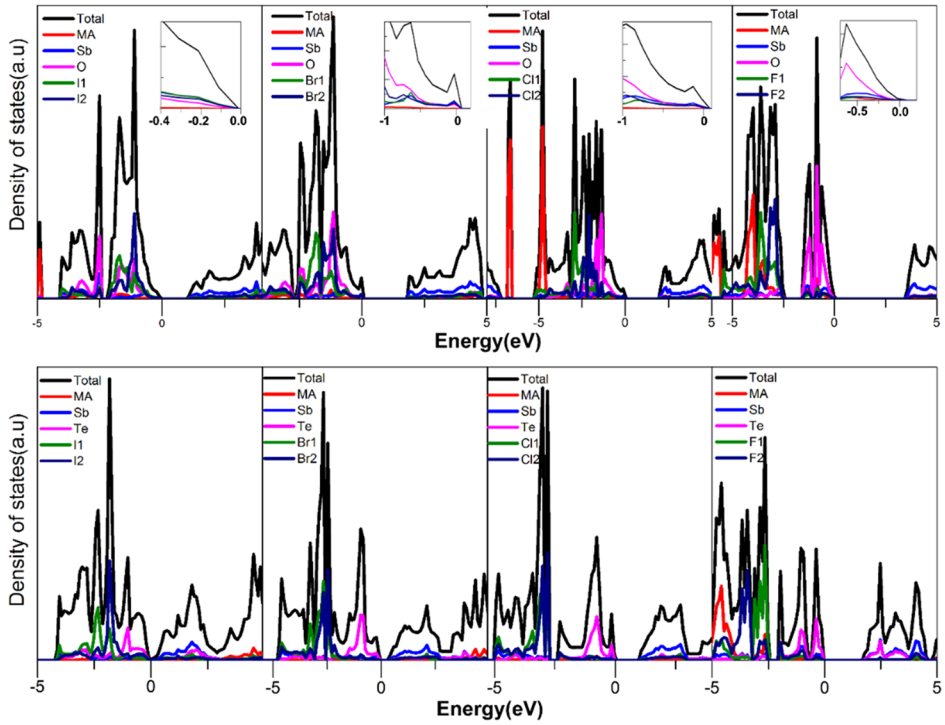

Figure 4. Density of states (DOS) and projected density of states (PDOS) of MASbOX″$_2$ and MASbTeX″$_2$. The inset shows the DOS and PDOS near the valence band maximum (VBM).

with a band gap of less than 5 eV. Although A cations do not directly influence the band gap due to little contribution to the electron orbital distribution at the band gap edge as discussed in the following, they can modify the lattice constant, and the band gap increases with an expansion of the lattice. For example, as shown in Figure S1, for the class of $ABOI_2$ (A = Cs^+, MA^+, FA^+; B = In^{3+}, Sb^{3+}, Bi^{3+}), the crystal volume follows the order of Cs < FA < MA, and the band gap increases with the increase in volume. Similar to the band gap trend for pure halide perovskites, the band gap value also increases when X″ changes from I to Br, Cl, and F (from top to bottom in the panel). In addition, the band gap decreases when the X′ part changes from O to S, Se, and Te (from left to right in the panel). To further understand the synergistic influence of the two different kinds of anions on the band gap, we calculated the relationship between the gaps and the geometrical average of the electronegativity of the constituent anions.

The Cs systems are not considered because most of their band gaps are nearly zero. Figure 3 shows the influence of total anion electronegativity on band gaps for the MA and FA systems. The electronegativity values on the abscissa range from small to large with labels of the corresponding anion groups. It was found that for most mixed-anion perovskites, especially MASbX′X″$_2$, there was a linear relationship between the band gap and the average electronegativity. The band gap increases with an increase in the electronegativity of anions, which is consistent with the trend in halogen perovskites.[28] It is notable that the scattering of FAGaX′X″$_2$ is completely

https://dx.doi.org/10.1021/acs.jpcc.9b10217
J. Phys. Chem. C 2020, 124, 1303−1308

chaotic due to the destruction of the perovskite phase structures (Figure S2).

Subsequently, we calculated the density of states (DOS) of a series of $MASbX'X''_2$ to more thoroughly understand the roles of chalcogen and halogen elements. DOS analysis is helpful for resolving the contribution of constituent elements on band-edge states that determine the band gap of the system. Figure 4 shows the DOS and PDOS of $MASbX'X''_2$. The results demonstrate that the conduction band minimum (CBM) is mainly contributed by Sb ions and that the valence band maximum (VBM) is mainly contributed by anions. Furthermore, MA makes a slight contribution to the band-edge states, corresponding to the role of A cations for lead perovskites. To resolve the effect of anions, we focused on the contribution of anions on the valence band maximum. For $MASbTeX''_2$, the VBM is mainly contributed by the chalcogen element Te, and halogen elements make slight contributions. However, for $MASbOI_2$, the result is the opposite, and the major contribution of the VBM derives from I. The electron affinity alignment of anions studied in this work is summarized in Figure S3. The electron affinity follows the order of Te < I < Br < Cl < O. In combination with the above PDOS analysis for Te and O compounds, we found that anions with lower electron affinity make greater contributions to the VBM. Further support was provided by a correlation plot of the contribution ratio of O and X″ (X″ = F, Cl, Br, and I) to the VBM as a function of the electron affinity of halogen elements for $MASbOX''_2$ (Figure S4a). The contribution of X″ to the CBM increases as the electron affinity decreases. Therefore, it is reasonable to establish a correlation of decreasing electron affinity of anions with increasing contributions to the VBM for mixed-anion perovskites. In addition, for $MASbX'X''_2$, there are two kinds of X″ atoms that have different bond lengths with Sb (Figure S4b). As shown in Figure 4, the contributions of such X″ atoms are different, suggesting that bond length is also a parameter concerning the influence of anions on the band-edge states.

Finally, we screened out the perovskite structure that meets requirements from the 192 lead-free mixed-anion perovskites. Although the theoretical optimal band gap for high photovoltaic energy conversion efficiency is 1.34 eV,[30] the screening criteria in this work were set to a range from 1.24 to 1.44 eV. Furthermore, according to Goldschmidt's rule, for a 3D perovskite with a formula of ABX_3, the ionic radii of A, B, and X need to meet the condition of the tolerance factor $t = \frac{(R_A + R_X)}{\sqrt{2}(R_B + R_X)}$ $(0.8 < t < 1.1)$ and the octahedral factor $\mu = \frac{R_B}{R_X}$ $(0.414 < \mu < 0.7)$.[31,32]

Table 1 summarizes the parameters of six perovskites with suitable band gaps. However, only perovskite $CsInOBr_2$ can meet all the above screening conditions. The calculated electronic band structure (Figure S5) shows that $CsInOBr_2$ is a direct band gap semiconductor with both the conduction band minimum (CBM) and valence band maximum (VBM) being located at the Γ point. To evaluate whether the candidate may theoretically form, we calculated the formation energy of $CsInOBr_2$, and the value was −1.32 eV/atom, suggesting that $CsInOBr_2$ might be obtained from synthesis experiments. Subsequently, we calculated the decomposition energy by considering three possible decomposition pathways as follows[43]

$$CsInOBr_2 \rightarrow CsBr + 1/2\ O_2 + InBr \quad (4)$$

Table 1. Summary of the Related Parameters—Band Gap, Tolerance Factor (t), and Octahedral Factor (μ)—of the Selected Lead-Free Perovskites

compound	band gap (eV)	t	μ
$FABiSeF_2$	1.43	1.19	0.65
$MABiTeBr_2$	1.34	1.14	0.60
$FAGaSBr_2$	1.41	1.52	0.48
$FAGaSeF_2$	1.28	1.49	0.46
$FAInSI_2$	1.41	1.35	0.57
$FAInTeI_2$	1.27	1.30	0.51
$CsInOBr_2$	1.30	1.02	0.69
$FAInOI_2$	1.43	1.43	0.69

$$CsInOBr_2 \rightarrow 1/6\ (3Cs_2O + In_2O_3 + 4InBr_3) \quad (5)$$

$$CsInOBr_2 \rightarrow CsBr + 1/3\ In_2O_3 + 1/3\ InBr_3 \quad (6)$$

The first two pathways show positive values of 0.26 and 0.23 eV/atom, respectively. Also, the third one exhibits a small negative value of −0.08 eV/atom, indicating that $CsInOBr_2$ is mildly metastable[44,45] and may be synthesized experimentally under equilibrium conditions. In addition, we performed ab initio molecular dynamics (AIMD) simulations to evaluate the thermal stability of $CsInOBr_2$. As shown in Figure S6, the evolutions of total energies are oscillating within a very narrow range of 1 ps, indicating that $CsInOBr_2$ is thermally stable.

CONCLUSIONS

We calculated 192 lead-free anion-mixed perovskite materials and obtained a promising candidate $CsInOBr_2$ with a suitable band gap of 1.30 eV for photovoltaic applications. For mixed-anion perovskites, the band gap increased with an increase in the electronegativity of the anions. Cations mainly contributed to the CBM, and the contribution of anions to the VBM depended on the electron affinity and the B−X bond lengths. Our work provides a new direction to explore stable, lead-free perovskite materials for photovoltaic applications.

ASSOCIATED CONTENT

Supporting Information

The Supporting Information is available free of charge at https://pubs.acs.org/doi/10.1021/acs.jpcc.9b10217.

The electron affinity of the anions studied in this work; Electronic bandgap structure, AIMD stimulations and formation energy of $CsInOBr_2$; Detailed calculated bandgap results and ion radiuses of the mixed-anion perovskites studied in this work (PDF)

AUTHOR INFORMATION

Corresponding Author

Lei Sun − *Shandong University, Qingdao, People's Republic of China*; Email: slei@sdu.edu.cn

Other Authors

Xin Mao − *Dalian Institute of Chemical Physics, Dalian, People's Republic of China, and University of the Chinese Academy of Sciences, Beijing, People's Republic of China*

Ke-Li Han − *Dalian Institute of Chemical Physics, Dalian, People's Republic of China*; orcid.org/0000-0001-9239-1827

https://dx.doi.org/10.1021/acs.jpcc.9b10217
J. Phys. Chem. C 2020, 124, 1303−1308

Wei-Qiao Deng − *Shandong University, Qingdao, People's Republic of China;* orcid.org/0000-0002-3671-5951

Complete contact information is available at: https://pubs.acs.org/10.1021/acs.jpcc.9b10217

Notes

The authors declare no competing financial interest.

■ ACKNOWLEDGMENTS

This work was supported by the National Key Research and Development Program of China (no. 2017YFA0204800), the National Natural Science Foundation of China (nos. 21525315, 21533010, 21833009, and 91333116), and the Fundamental Research Funds of Shandong University (no. 2019HW016).

■ REFERENCES

(1) National Renewable Energy Laboratory. *Best Research-Cell Efficiencies*; https://www.nrel.gov/pv/assets/pdfs/best-research-cell-efficiencies.20190923.pdf.

(2) Luo, S.; Daoud, W. A. Recent progress in organic-inorganic halide perovskite solar cells: mechanisms and material design. *J. Mater. Chem. A* **2015**, *3*, 8992−9010.

(3) Kojima, A.; Teshima, K.; Shirai, Y.; Miyasaka, T. Organometal Halide Perovskites as Visible-Light sensitizers for Photovoltaic Cells. *J. Am. Chem. Soc.* **2009**, *131*, 6050−6051.

(4) Jeon, N. J.; Noh, J. H.; Yang, W. S.; Kim, Y. C.; Ryu, S.; Seo, J.; Seok, S. I. Compositional engineering of perovskite materials for high-performance solar cells. *Nature* **2015**, *517*, 476.

(5) Liu, M.; Johnston, M. B.; Snaith, H. J. Efficient planar heterojunction perovskite solar cells by vapour deposition. *Nature* **2013**, *501*, 395−398.

(6) Green, M. A.; Ho-Baillie, A.; Snaith, H. J. The emergence of perovskite solar cells. *Nat. Photonics* **2014**, *8*, 506−514.

(7) Lee, M. M.; Teuscher, J.; Miyasaka, T.; Murakami, T. N.; Snaith, H. J. Efficient Hybrid Solar Cells Based on Meso-Superstructured Organometal Halide Perovskites. *Science* **2012**, *338*, 643−647.

(8) Yang, W. S.; Park, B.-W.; Jung, E. H.; Jeon, N. J.; Kim, Y. C.; Lee, D. U.; Shin, S. S.; Seo, J.; Kim, E. K.; Noh, J. H.; Seok, S. I. Iodide management in formamidinium-lead-halide-based perovskite layers for efficient solar cells. *Science* **2017**, *356*, 1376−1379.

(9) Giustino, F.; Snaith, H. J. Toward Lead-Free Perovskite Solar Cells. *ACS Energy Lett.* **2016**, *1*, 1233−1240.

(10) McClure, E. T.; Ball, M. R.; Windl, W.; Woodward, P. M. Cs_2AgBiX_6(X = Br, Cl): New Visible Light Absorbing, Lead-Free Halide Perovskite Semiconductors. *Chem. Mater.* **2016**, *28*, 1348−1354.

(11) Noel, N. K.; Stranks, S. D.; Abate, A.; Wehrenfennig, C.; Guarnera, S.; Haghighirad, A.-A.; Sadhanala, A.; Eperon, G. E.; Pathak, S. K.; Johnston, M. B.; Petrozza, A.; Herz, L. M.; Snaith, H. J. Lead-free organic-inorganic tin halide perovskites for photovoltaic applications. *Energy Environ. Sci.* **2014**, *7*, 3061−3068.

(12) Stoumpos, C. C.; Malliakas, C. D.; Kanatzidis, M. G. Semiconducting Tin and Lead Iodide Perovskites with Organic Cations: Phase Transitions, High Mobilities, and Near-Infrared Photoluminescent Properties. *Inorg. Chem.* **2013**, *52*, 9019−9038.

(13) Yang, S.; Fu, W.; Zhang, Z.; Chen, H.; Li, C.-Z. Recent advances in perovskite solar cells: efficiency, stability and lead-free perovskite. *J. Mater. Chem. A* **2017**, *5*, 11462−11482.

(14) Filip, M. R.; Hillman, S.; Haghighirad, A. A.; Snaith, H. J.; Giustino, F. Band Gaps of the Lead-Free Halide Double Perovskites $Cs_2BiAgCl_6$ and $Cs_2BiAgBr_6$ from Theory and Experiment. *J. Phys. Chem. Lett.* **2016**, *7*, 2579−2585.

(15) Hoefler, S. F.; Trimmel, G.; Rath, T. Progress on lead-free metal halide perovskites for photovoltaic applications: a review. *Monatsh. Chem.* **2017**, *148*, 795−826.

(16) Luo, J.; Wang, X.; Li, S.; Liu, J.; Guo, Y.; Niu, G.; Yao, L.; Fu, Y.; Gao, L.; Dong, Q.; Zhao, C.; Leng, M.; Ma, F.; Liang, W.; Wang, L.; Jin, S.; Han, J.; Zhang, L.; Etheridge, J.; Wang, J.; Yan, Y.; Sargent, E. H.; Tang, J. Efficient and stable emission of warm-white light from lead-free halide double perovskites. *Nature* **2018**, *563*, 541−545.

(17) Chen, M.; Ju, M.-G.; Garces, H. F.; Carl, A. D.; Ono, L. K.; Hawash, Z.; Zhang, Y.; Shen, T.; Qi, Y.; Grimm, R. L.; Pacifici, D.; Zeng, X. C.; Zhou, Y.; Padture, N. P. Highly stable and efficient all-inorganic lead-free perovskite solar cells with native-oxide passivation. *Nat. Commun.* **2019**, *10*, 16.

(18) Hao, F.; Stoumpos, C. C.; Cao, D. H.; Chang, R. P. H.; Kanatzidis, M. G. Lead-free solid-state organic-inorganic halide perovskite solar cells. *Nat. Photonics* **2014**, *8*, 489−494.

(19) Xiao, Z.; Meng, W.; Wang, J.; Mitzi, D. B.; Yan, Y. Searching for promising new perovskite-based photovoltaic absorbers: the importance of electronic dimensionality. *Mater. Horiz.* **2017**, *4*, 206−216.

(20) Liao, Y.; Liu, H.; Zhou, W.; Yang, D.; Shang, Y.; Shi, Z.; Li, B.; Jiang, X.; Zhang, L.; Quan, L. N.; Quintero-Bermudez, R.; Sutherland, B. R.; Mi, Q.; Sargent, E. H.; Ning, Z. Highly Oriented Low-Dimensional Tin Halide Perovskites with Enhanced Stability and Photovoltaic Performance. *J. Am. Chem. Soc.* **2017**, *139*, 6693−6699.

(21) Yokoyama, T.; Cao, D. H.; Stoumpos, C. C.; Song, T.-B.; Sato, Y.; Aramaki, S.; Kanatzidis, M. G. Overcoming Short-Circuit in Lead-Free $CH_3NH_3SnI_3$ Perovskite Solar Cells via Kinetically Controlled Gas-Solid Reaction Film Fabrication Process. *J. Phys. Chem. Lett.* **2016**, *7*, 776−782.

(22) Krishnamoorthy, T.; Ding, H.; Yan, C.; Leong, W. L.; Baikie, T.; Zhang, Z.; Sherburne, M.; Li, S.; Asta, M.; Mathews, N.; Mhaisalkar, S. G. Lead-free germanium iodide perovskite materials for photovoltaic applications. *J. Mater. Chem. A* **2015**, *3*, 23829−23832.

(23) Jana, M. K.; Janke, S. M.; Dirkes, D. J.; Dovletgeldi, S.; Liu, C.; Qin, X.; Gundogdu, K.; You, W.; Blum, V.; Mitzi, D. B. Direct-Bandgap 2D Silver-Bismuth Iodide Double Perovskite: The Structure-Directing Influence of an Oligothiophene Spacer Cation. *J. Am. Chem. Soc.* **2019**, *141*, 7955−7964.

(24) Khalfin, S.; Bekenstein, Y. Advances in lead-free double perovskite nanocrystals, engineering band-gaps and enhancing stability through composition tunability. *Nanoscale* **2019**, *11*, 8665−8679.

(25) Sun, Y.-Y.; Shi, J.; Lian, J.; Gao, W.; Agiorgousis, M. L.; Zhang, P.; Zhang, S. Discovering lead-free perovskite solar materials with a split-anion approach. *Nanoscale* **2016**, *8*, 6284−6289.

(26) Nie, R.; Mehta, A.; Park, B.-w.; Kwon, H.-W.; Im, J.; Seok, S. I. Mixed Sulfur and Iodide-Based Lead-Free Perovskite Solar Cells. *J. Am. Chem. Soc.* **2018**, *140*, 872−875.

(27) Jiang, L.; Wu, T.; Sun, L.; Li, Y.-J.; Li, A.-L.; Lu, R.-F.; Zou, K.; Deng, W.-Q. First-Principles Screening of Lead-Free Methylammonium Metal Iodine Perovskites for Photovoltaic Application. *J. Phys. Chem. C* **2017**, *121*, 24359−24364.

(28) Castelli, I. E.; García-Lastra, J. M.; Thygesen, K. S.; Jacobsen, K. W. Bandgap calculations and trends of organometal halide perovskites. *APL Mater.* **2014**, *2*, 081514.

(29) Castelli, I. E.; Olsen, T.; Datta, S.; Landis, D. D.; Dahl, S.; Thygesen, K. S.; Jacobsen, K. W. Computational screening of perovskite metal oxides for optimal solar light capture. *Energy Environ. Sci.* **2012**, *5*, 5814−5819.

(30) Polman, A.; Knight, M.; Garnett, E. C.; Ehrler, B.; Sinke, W. C. Photovoltaic Materials: Present Efficiencies and Future Challenges. *Science* **2016**, *352*, aad4424.

(31) Saliba, M.; Matsui, T.; Domanski, K.; Seo, J.-Y.; Ummadisingu, A.; Zakeeruddin, S. M.; Correa-Baena, J.-P.; Tress, W. R.; Abate, A.; Hagfeldt, A.; Grätzel, M. Incorporation of rubidium cations into perovskite solar cells improves photovoltaic performance. *Science* **2016**, *354*, 206−209.

(32) Shi, Z.; Guo, J.; Chen, Y.; Li, Q.; Pan, Y.; Zhang, H.; Xia, Y.; Huang, W. Lead-Free Organic-Inorganic Hybrid Perovskites for

Photovoltaic Applications: Recent Advances and Perspectives. *Adv. Mater.* **2017**, *29*, 1605005.
(33) Kresse, G.; Furthmüller, J. Efficiency of ab-initio total energy calculations for metals and semiconductors using a plane-wave basis set. *Comput. Mater. Sci.* **1996**, *6*, 15−50.
(34) Kresse, G.; Furthmüller, J. Efficient iterative schemes for *ab initio* total-energy calculations using a plane-wave basis set. *Phys. Rev. B* **1996**, *54*, 11169−11186.
(35) Blöchl, P. E. Projector augmented-wave method. *Phys. Rev. B* **1994**, *50*, 17953−17979.
(36) Amat, A.; Mosconi, E.; Ronca, E.; Quarti, C.; Umari, P.; Nazeeruddin, M. K.; Grätzel, M.; De Angelis, F. Cation-Induced Band-Gap Tuning in Organohalide Perovskites: Interplay of Spin-Orbit Coupling and Octahedra Tilting. *Nano Lett.* **2014**, *14*, 3608−3616.
(37) Perdew, J. P. Density Functional Theory and the Band Gap Problem. *Int. J. Quantum Chem.* **1985**, *28*, 497−523.
(38) Bernardi, M.; Grossman, J. C. Computer calculations across time and length scales in photovoltaic solar cells. *Energy Environ. Sci.* **2016**, *9*, 2197−2218.
(39) Mortensen, J. J.; Hansen, L. B.; Jacobsen, K. W. Real-space grid implementation of the projector augmented wave method. *Phys. Rev. B* **2005**, *71*, No. 035109.
(40) Enkovaara, J.; Rostgaard, C.; Mortensen, J. J.; Chen, J.; Dułak, M.; Ferrighi, L.; Gavnholt, J.; Glinsvad, C.; Haikola, V.; Hansen, H. A.; Kristoffersen, H. H.; Kuisma, M.; Larsen, A. H.; Lehtovaara, L.; Ljungberg, M.; Lopez-Acevedo, O.; Moses, P. G.; Ojanen, J.; Olsen, T.; Petzold, V.; Romero, N. A.; Stausholm-Møller, J.; Strange, M.; Tritsaris, G. A.; Vanin, M.; Walter, M.; Hammer, B.; Häkkinen, H.; Madsen, G. K. H.; Nieminen, R. M.; Nørskov, J. K.; Puska, M.; Rantala, T. T.; Schiøtz, J.; Thygesen, K. S.; Jacobsen, K. W. Electronic structure calculations with GPAW: a real-space implementation of the projector augmented-wave method. *J. Phys.: Condens. Matter* **2010**, *22*, 253202.
(41) Gritsenko, O.; van Leeuwen, R.; van Lenthe, E.; Baerends, E. J. Self-Consistent Approximation to the Kohn-Sham Exchange Potential. *Phys. Rev. A* **1995**, *51*, 1944−1954.
(42) Kuisma, M.; Ojanen, J.; Enkovaara, J.; Rantala, T. T. Kohn-Sham Potential with Discontinuity for Band Gap Materials. *Phys. Rev. B* **2010**, *82*, 115106.
(43) Xiao, Z.; Du, K.-Z.; Meng, W.; Wang, J.; Mitzi, D. B.; Yan, Y. Intrinsic Instability of $Cs_2In(I)M(III)X_6$ (M = Bi, Sb; X = Halogen) Double Perovskites: A Combined Density Functional Theory and Experimental Study. *J. Am. Chem. Soc.* **2017**, *139*, 6054−6057.
(44) Castelli, I. E.; Olsen, T.; Datta, S.; Landis, D. D.; Dahl, S.; Thygesen, K. S.; Jacobsen, K. W. Computational Screening of Perovskite Metal Oxides for Optimal Solar Light Capture. *Energy Environ. Sci.* **2012**, *5*, 5814−5819.
(45) Zhang, Y.-Y.; Chen, S.; Xu, P.; Xiang, H.; Gong, X.-G.; Walsh, A.; Wei, S.-H. Intrinsic Instability of the Hybrid Halide Perovskite Semiconductor $CH_3NH_3PbI_3$. *Chin. Phys. Lett.* **2018**, *35*, No. 036104.

https://dx.doi.org/10.1021/acs.jpcc.9b10217
J. Phys. Chem. C 2020, 124, 1303−1308